3134.5-P

RESEARCH ON METASTABLE SPECIES IN ATOMIC AND MOLECULAR BEAMS PRODUCED BY CHARGE TRANSFER
Tasks I, II, and III

AD 664169

Sponsored by:

ADVANCED RESEARCH PROJECTS AGENCY
PROJECT DEFENDER
ARPA ORDER NO. 553

Monitored by:

U.S. ARMY RESEARCH OFFICE — DURHAM
CONTRACT DA-31-124-ARO-D-446

STANFORD RESEARCH INSTITUTE

MENLO PARK, CALIFORNIA ⊕SRI

RESEARCH ON METASTABLE SPECIES IN ATOMIC
AND MOLECULAR BEAMS PRODUCED BY CHARGE TRANSFER
Tasks I, II, and III

By: M. HOLLSTEIN,   D. C. LORENTS,   J. R. PETERSON,   AND   R. A. YOUNG

SRI Project PAU-5962

Copy No. 1 7

BLANK PAGE

SYNOPSIS

Excited species and excited state reactions involving radiative and metastable states of atmospheric species play an important role in reentry physics. Progress in laboratory studies leading to the understanding of these reactions and the determination of the pertinent reaction rates is reported.

Near-resonant electron capture reactions are being used to produce beams of long-lived excited atoms and molecules (metastables) suitable for studies of important collision processes of such species. The research has progressed sufficiently to allow the measurement of cross sections as a function of kinetic energy for metastable deactivation processes. Reactions in which the deactivation was dominated by Penning ionization or by symmetric energy transfer were chosen for study so that cross sections for these particular processes could be obtained.

Studies of the optical radiation emitted from states excited by electron capture collisions have also provided useful results. In particular, cross sections for electron capture into the $v' = 0, 1, 2$ vibrational levels of the $C^3\Pi_u$ state of N_2 have been measured as a function of energy for the reactants $N_2^+ + K$, by observing the second positive radiation. Since this state decays via the $B^3\Pi_g$ state to the metastable $A^3\Sigma_u$ state, a beam of N_2 molecules in the A state results, whose concentration can be inferred from the cascade radiation. These studies have demonstrated that cross section measurements on collision processes involving metastable N_2 can now be carried out.

Measurements of the gas phase quenching and reactions of $O(^1D)$ by O_2, N_2O, CO, CO_2, and H_2 are nearing completion. Various experimental and

interpretative difficulties with these experiments have been overcome and definitive results are now assured.

The excitation and de-excitation of $O_2(b^1\Sigma^+)$, $N_2(A^3\Sigma_u^+)$, and $O(^1S)$ in a weak discharge are being successfully studied. Results are in the final stages of verification. Energy transfer from $N_2(A^3\Sigma_u^+)$ to N_2 that produces $N_2(C^3\Pi)$ and $N_2(B^3\Pi)$ has been observed and is in an interpretative stage of analysis.

The study of free radical interaction with atomic O and N are in an initial stage of development.

CONTENTS

INTRODUCTION

It is clear that excited atomic and molecular species play an important role in reentry physics. The short-lived excited species manifest themselves by the visible radiation they emit in the shock wave and the wake of a reentering body. Much of the excitation energy, however, remains imprisoned in the hot gas for a long time, either because it is absorbed and re-emitted rapidly or because it is trapped in nonradiating states. This trapped energy is released through a variety of energy transfer reactions that influence the chemistry of the development and relaxation of a reentry shock wave as well as its radiative signature. To understand the role of this excitation energy in shock wave phenomena, a knowledge of the direct interactions between excited and ground state particles and of the radiation transfer is needed. Cross sections or rate constants of the most important energy transfer reactions involving excited species are needed along with radiative transition probabilities.

Two lines of work are currently being pursued that bear directly on the important problem of the role of excited species in reentry phenomena. In Task I, beam methods have been developed to study energy transfer processes of metastable excited atoms and molecules in collisions with ground state species. In Task II, flowing afterglow techniques and optical detection of photolysis fragments are used to study exothermic chemiluminescent reaction mechanisms in excited atmospheric gases.

The objective of Task III is to apply sensitive optical methods developed for laboratory studies to spectral measurements of the radiation associated with the high altitude release of barium.

1

Progress in each of these tasks is described in this report. Task I has been carried out by M. Hollstein, D. C. Lorents, J. R. Peterson, and A. Salop. Tasks II and III are under the direction of R. A. Young.

I BEAM STUDIES OF EXCITED SPECIES

Since the last report the research on metastable beams has proceeded
along two lines. First, studies of the optical radiation resulting from
charge exchange reactions in which there are near resonances with excited
states have continued. This work is described below in Section I-B.
Second, in another apparatus charge exchange has been used to produce
beams of neutrals that contain a large fraction of metastables. Using
these beams, studies of deactivation processes of the metastables have
begun. A detailed description of this work is given in Section I-A.

A. Deactivation Cross Sections of Metastables

1. Production of a Metastable Beam

The process of resonant or near-resonant electron capture by ions
passing through a target gas has been used to produce beams of metastables
sufficiently intense for collision studies.[1,2] Beams of excited He, Ne,
and N_2 have been obtained in the energy range from 40 to 1000 eV. To
produce a metastable beam, an ion beam of the desired energy and species
is initially formed. The ions pass through a charge transfer cell where
an alkali vapor is maintained at a constant vapor pressure of about 10^{-4}
torr. The two metastable levels in a noble gas atom lie about 3 to 4 eV
below the ionization limit. The process of charge transfer populates
predominantly those levels of the noble gas atom for which

$$E_A \cong E_B - E^*$$

where E_A is ionization energy of the alkali, E_B is the ionization energy
of the excited noble gas, and E^* is the excitation energy of the noble

3

gas. This relation is valid for the metastable levels as well as optically allowed levels. The decaying states lead to a component of ground state atoms in our beam. Because of the large values[3] of the charge transfer cross section (thus large impact parameters) and the small energy loss for small angle scattering (characteristic of large impact parameters), the energy of the neutralized particles in the forward direction is essentially the same as the incident ion energy.

2. Apparatus

a. Vacuum Chambers

The apparatus, shown in Fig. 1, consists of three valve-separated vacuum chambers. One section contains the source and the magnet poles of a magnetic mass spectrometer. This section is pumped by a 4-inch oil diffusion pump trapped by a refrigerated baffle. The background pressure is 5×10^{-7} torr. The middle section of the apparatus contains the charge transfer cell. This section is also pumped by a 4-inch oil diffusion pump trapped by a refrigerated baffle. The background pressure is 10^{-6} torr. The last container is the interaction cell. It is pumped by a 6-inch oil diffusion pump and trapped by a liquid nitrogen baffle, and the background pressure is $<10^{-7}$ torr.

b. Ion Source and Beam Focusing

The ion source is a nonself-sustained discharge source that has been used in this laboratory in previous experiments.[4] The energy of the ions can be varied between 25 and 1500 eV. The energy spread is about 2 eV over the entire energy range (full width at half maximum). The ions are extracted from the discharge through a 5/16-inch hole and accelerated by a three-element, 3-lens system. Two condensers, perpendicular to each other, allow adjustment of the direction.

4

Legend:

- ❶ Ion source
- ❷ Lens system & deflecting plates
- ❸ Magnet
- ❹ Lens system (retarding focussing)
- ❺,❻ Shut-off valves
- ❼,❽ Gas inlets
- ❾ Charge transfer oven
- ❿ Cooling
- ⓫,⓬ Apertures
- ⓭ Deflecting plates
- ⓮ Interaction cell
- ⓯ Surface detector
- ⓰ Op. amp. 1, 2, & 3
- ⓱ Teflon
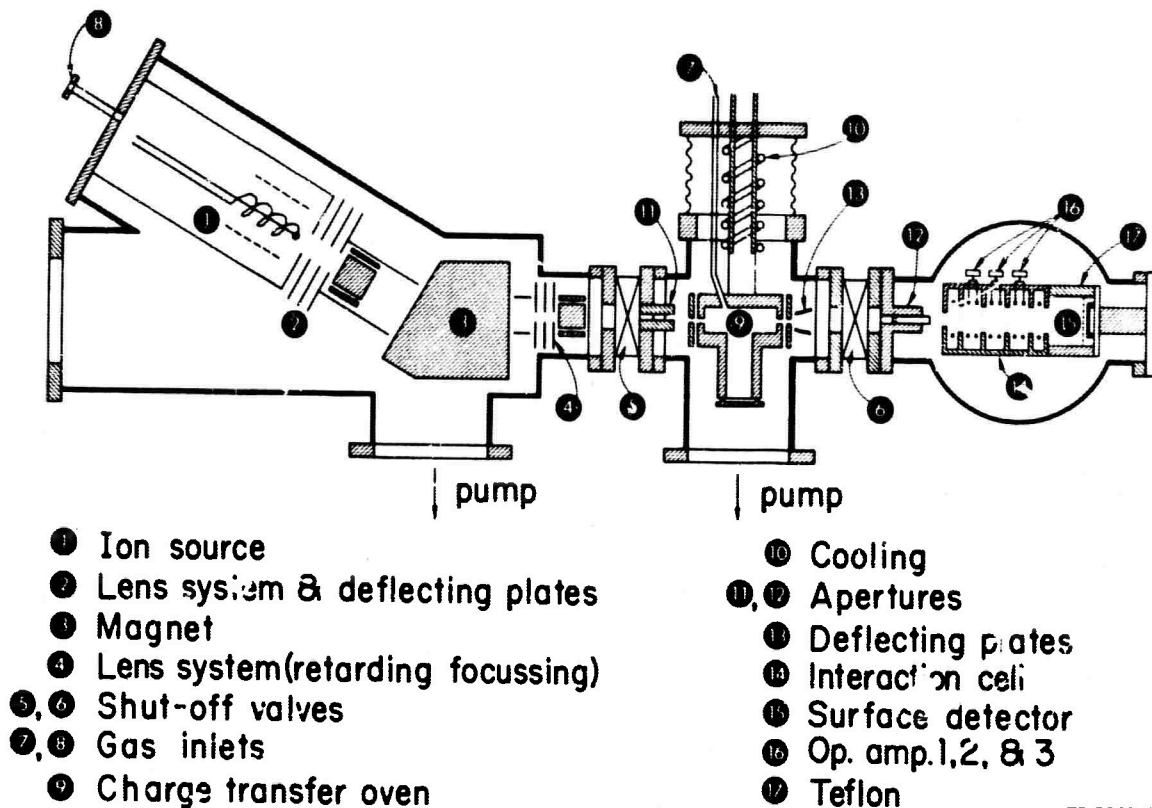
TD-5962-13

FIG. 1 SCHEMATIC DIAGRAM OF THE APPARATUS

c. Magnetic Spectrometers and Additional Focusing

After it leaves the source system, the beam is deflected 30° by means of a homogeneous magnetic field. The magnetic spectrometer has a resolution of about 20 and the transmission is high. It serves the purpose of clearing the beam of undesired particles, produced in the source, without much loss of intensity. After passing the magnet the beam can be refocused and realigned by an einzel lens and deflector plates.

d. Charge Transfer Cell

The beam enters the charge transfer region through an aperture tube 1/4 inch in diameter and 2 inches long. A T-shaped alkali oven forms the transfer cell. The stainless steel oven is enclosed in a 3/16-inch copper cover to increase the thermal conductivity. The oven is heated

5

electrically by several tungsten heating coils. The temperature is meas-
ured by an iron-constantan thermocouple. To conserve alkali, the oven
can be cooled quickly by establishing a thermal contact between it and a
water-cooled 1-inch-diameter copper rod. The beam enters and leaves the
oven through 3/16-inch-diameter holes. The length of the oven chamber
(transfer cell) is 2-1/2 inches. Cooled caps at both ends of the cell
collect most of the outcoming thermal alkali atoms during the measurement.
Gas can be let into the transfer cell through a 1/8-inch-diameter tube,
which leads from the oven to the outside of the apparatus. Deflector plates
near the exit hole of the oven remove all remaining charged particles from
the beam. Through another aperture tube (3/16 inch in diameter, 2 inches
long), the neutralized part of the beam enters the interaction chamber.

e. Interaction Chamber and Detector

The interaction chamber can be filled with different gases by
means of a leak valve. The pressure is measured in the high vacuum range
(10^{-9} to 10^{-4} torr) with a Bayard Alpert-ionization gauge and in the range
10^{-5} to 1 torr with a Baratron capacitance manometer.

As the beam penetrates the gas in the interaction cell, some
ions are produced with energies less than a few eV. The detecting device
collects the ions generated in definite segments of the beam path. It
consists of a five-cavity system that is symmetric about the beam axis
(see Fig. 2). The cell is made of aluminum and is coated with aquadag on
surfaces exposed to the beam. The smaller outer cavities serve only to
isolate the inner ones from end effects. The outer cells each contain
one insulated wire ring, the inner cells each contain two. These are the
collecting electrodes. During the measurement the rings are at zero
potential, while the aluminum cell is at a potential of +60 volts. The
inner cavities are electrically separated by grids that cover the 2-inch-
diameter openings between cells. The transparency of the grids is 99%.

6
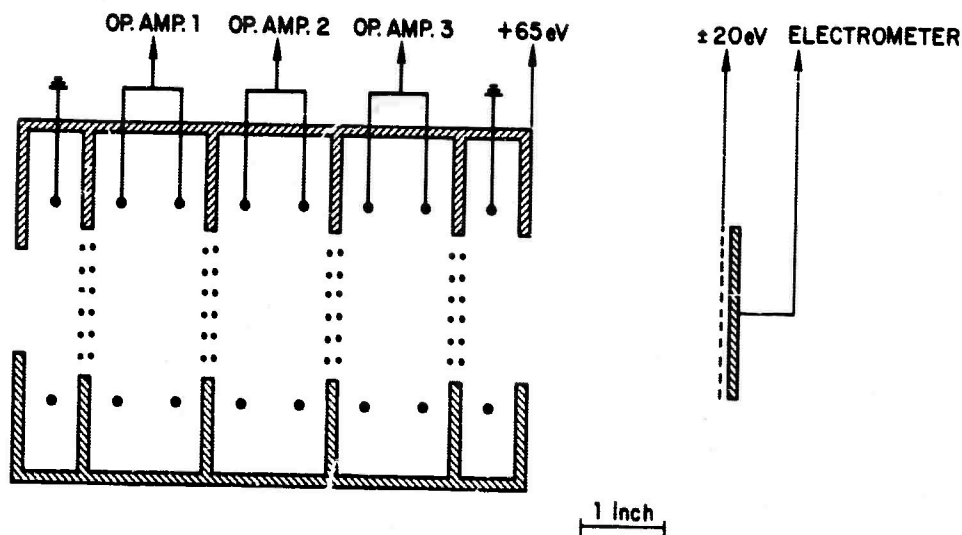
FIG. 2   DEACTIVATION CELL

1 Inch

TB-5962-27

The geometry, together with the applied potentials, produces a potential valley for ions inside each cavity, the lowest potential being at the surface of the rings themselves. The ions are trapped in the cavities and collected by the rings. The collection length is well defined and is the same for all the inner cavities. Nearly 100% collection efficiency is attained, and photon-induced background is kept very low due to the small surface area of the rings. The ion currents collected in the three inner cavities are measured by three operational amplifiers (AD029). With an input impedance of 10^9 Ω, currents of 10^{-12} amp can be measured. The amplifiers are mounted inside the vacuum chamber to reduce pickup noise. An electronic scanning device records the currents and the pressure on magnetic tape.

The beam particles that pass through the cavity system finally hit a surface detector. This simple device consists of an aluminum disk 2 inches in diameter, covered with aquadag; a high transparency tungsten

7

grid is placed in front of it. With the grid at +20 volts, electrons ejected by beam particles leave the detector plate. An electrometer connected to this plate reads a positive current proportional to the beam intensity. This detector is used as a beam monitor.

3. Beam Interactions

a. Charge Transfer

The metastable beam intensity is determined by three processes:

(a) The neutralization of the ions.

(b) The scattering of the ions.

(c) The scattering of the neutralized particles.

If i_+^0 is the intensity of the incident ion beam, the intensity i_o^0 of the neutralized part in the forward direction after passing the transfer region is given by[5]

$$i_o^0 = \frac{Q_{tr}}{Q_i - Q_o + Q_{tr}} i_+^0 \exp(-nQ_o \ell) \left[1 - \exp(-n\ell[Q_i - Q_o + Q_{tr}]) \right] \qquad (1)$$

where Q_{tr}, Q_i, and Q_o are the cross sections connected with the processes a, b, and c, ℓ is the length of the transfer region, and n is the density of the gas in this region.

The dependence of i_o^0 on density n, corresponding to temperature T of the oven, is shown in Fig. 3. With increasing density n or temperature T, the neutralized part rises to a maximum value of i_o^{max} at the density n_{max}. Because of an increasing amount of scattering at higher densities, the intensity of the neutral beam in the forward direction decreases for $n > n_{max}$. The measured curve can be well described by an equation like (1), but because of the large beam diameter (low angular resolution) no conclusions can be drawn from a fit between the experimental and calculated curve. For the measurements the oven was heated to the temperature at which neutralization has its maximum. The alkali used for the transfer process was potassium.
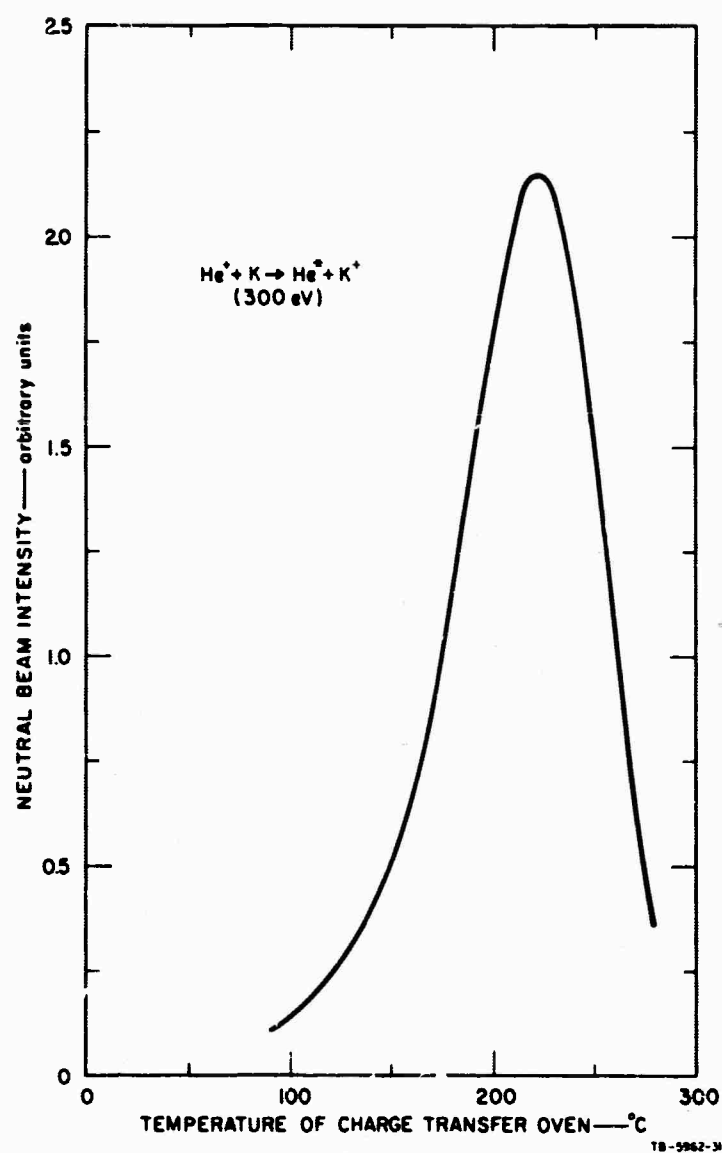
$He^+ + K \rightarrow He^* + K^+$
(300 eV)

FIG. 3 INCREASE OF THE NEUTRAL BEAM AS A FUNCTION
OF THE CHARGE TRANSFER OVEN TEMPERATURE

9

b. Interactions in the Detector Chamber

In the detector chamber the neutral beam particles A, consisting of excited species A^* and ground state species A^0, interact with the scattering gas B. For A^* the most important processes are

$$(a) \quad A^* + B \rightarrow A^* + B \qquad \text{(elastic scattering)}$$

$$(b) \quad A^* + B \rightarrow A + B^+ + e^- \qquad \text{(ionization of the target particle)}$$

$$(c) \quad A^* + B \rightarrow A^+ + e^- + B \qquad \text{(ionization of the beam particle)}$$

$$(d) \quad A^* + B \rightarrow A + B^* \qquad \text{(excitation transfer)}$$

If the excitation energy of A^* is larger than the ionization energy of B, excitation and ionization of B could occur in one process. Furthermore, if B is a molecule, it is possible that dissociation would accompany process b, c, or d.

For the component A^0 we have the corresponding processes a, b, and c, and the process of dissociation if B is a molecule. Although the ions, which are collected at the ring electrodes, are produced by processes b and c, their number is determined by the number of metastable and ground state species traversing each cell. If we include in a calculation of the currents $i_j (j = 1,2,3)$, collected in the cells 1, 2, and 3, all the mentioned processes, these currents are given as the solution of the differential equation.

$$di_j = i^*(x) \; Q_i^* \; ndx + i^0(x) \; Q_i^0 \; ndx$$

with

$$i^*(x) = i^*(0) \; \exp[-(Q_i^*+Q^*)] \; nx$$

and $i^0(x)$ given by

$$d[i^0(x)] = i^*(0) \; \exp[-(Q_i^*+Q^*)] \; nx \cdot (Q_i^*+Q^*) \; ndx - i^0(x) \cdot Q^0 \; ndx$$

10

where

x is distance from the entrance of the beam into the first cell along the beam path.

$i(x)$ is intensity of the beam at the distance x.

$i(0)$ is intensity of the beam at x = 0.

Q_i is cross section for ionization processes.

Q is cross section for all nonionizing deactivation processes.

* refers to the metastable particles.

° refers to the ground state particles.

n is density of the gas in the interaction cell.

With the integration limits x = 0 to ℓ for i_1, x = ℓ to 2ℓ for i_2, and x = 2ℓ to 3ℓ for i_3, the result is

$$i_j = i^*(0) \left[\frac{Q_i^*}{Q_i^* + Q^*} A_j(1-F) + \frac{Q_i^0}{Q_i^* + Q^* - Q^0} \left\{ \frac{Q_i^* + Q^*}{Q^0} B_j(1-G) - A_j(1-F) \right\} \right] + i^0(0) \frac{Q_i^0}{Q^0} B_j(1-G) \quad (2)$$

for j = 1,2,3 with

$A_1 = 1 \quad B_1 = 1$

$A_2 = F \quad B_2 = G$

$A_3 = F^2 \quad B_3 = G^2$

where

$F = \exp\left[-n(Q_i^* + Q^*)\ell \right]$

$G = \exp(-nQ^0 \ell)$

ℓ = length of each cavity cell

It should be noted that if any of the included processes consists of several mechanisms (e.g., excitation transfer into different states), the corresponding cross section in equation (2) has to be replaced by the sum of all cross sections for the different channels.

11

c. Calculation of Deactivation Cross Sections from the Measurements

Before cross sections are calculated, the following approximations for equation (2) are made:

$$Q^0 \ll Q_i^* + Q^* \quad ; \quad nQ^0 \ell \ll 1$$

Q^0 is the total elastic cross section for the particles in the ground state. Because of the large, grid-covered holes in the cavity cells, the contribution of elastic scattering to a decrease of the ground state component will be negligible. However, the inelastic processes connected with the metastable component are expected to be large. Both approximation assumptions are well justified for all the interaction partners under consideration.

Equation (2) is now reduced to

$$i_j = i^*(0) \left(\frac{Q_i^* - Q_i^0}{Q_i^* + Q^*} \cdot A_j(1-F) \right) + n \, Q_i^0 \left[i^*(0) + i^0(0) \right] \quad j = 1,2,3 \quad (3)$$

Although the cross sections $(Q_i^* + Q^*)$ could be obtained from these equations by introducing the measured values for the three currents, we simplify the expression for i_j by one more assumption. For the considered energy range, ionization cross sections Q_i^0 for ground state beam particles have been measured for some reaction par $\cdots$[6] and found to be $<10^{-16}$ cm^2. If we compare our results for Q_i^* with known values for Q_i^0, the relation

$$Q_i^0 \ll Q_i^*$$

is justified in most circumstances. Because the neutral component $i^0(0)$ is only a fraction of the metastable component, the assumption

$$Q_i^0 \left[i^0(0) + i^*(0) \right] \ll (Q_i^* + Q^*) \, i^*(0)$$

will be fulfilled.

12

In equation (3) we neglect the second term, and the final expression for the currents is

$$i_j = i^*(0) \frac{Q_i^* - Q_i^0}{Q_i^* + Q^*} \cdot A_j(1-F) \qquad j = 1,2,3$$

By taking the ratio of two successive currents, we get

$$\frac{i_1}{i_2} = \exp[+n(Q_i^*+Q^*)\ell] \quad \text{or} \quad \frac{i_1}{i_3} = \exp[2n(Q_i^*+Q^*)\ell]$$

The value of $(Q_i^*+Q^*)$ can be determined by either of these ratios. The sum of the cross sections is called the deactivation cross section Q_D for the metastable component of the beam interacting with the scattering gas.

Figure 4 shows measured values for a cross section at different cavity voltages. The plot indicates that between 50 and 80 volts the cross section is independent of the voltage within the error limits.
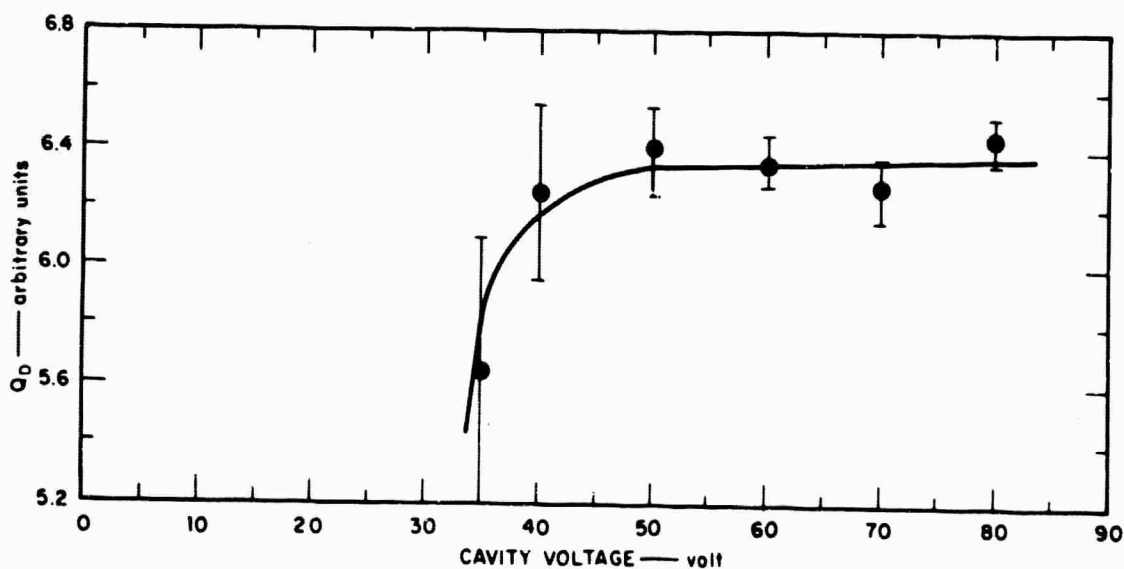
FIG. 4   DEPENDENCE OF THE DEACTIVATION CROSS SECTION ON THE CAVITY VOLTAGE

13

4. Results of the Measurements

The measurements have been carried out on two groups of reactions, one in which the metastable excitation energy is larger than the ionization of the target gas and another in which the target gas is the same species as the incident metastable.

Figure 5 shows the dependence of the deactivation cross section on the energy of the beam for reactions of the first group. The log-log plot of the dependence for each considered collision pair is a straight line and the slopes fall into two subgroups. In the $Ar^* + C_2H_2$ and $He^* + Ar$ cases the slope is 0.2 and in the $He^* + N_2$ and $He^* + C_2H_2$ cases the slope is 0.1. The distinguishing features of these subgroups appear to be that $Ar^* + C_2H_2$ and $He^* + Ar$ reactions involve a transition only to the ground state of the ion, whereas the second group involves transitions to several states. For the $Ar^* + C_2H_2$ interaction, the excitation energy of Ar^* only exceeds the ionization energy of C_2H_2 by 0.5 eV, so very little excitation can occur. In the case of $He^* + Ar$, Cermak[7] has shown for thermal collisions that the electrons absorb the excess energy (4.0 eV). A direct transition to the continuum from the temporary $HeAr^*$ molecular state formed probably occurs and ground state Ar^+ is produced.

In $He^* + N_2$, ionization will be the dominant process of deactivation, but there are a large number of channels available for the ionizing process $(Q_D \simeq \Sigma_i Q_i^*)$. The same consideration can be applied to the $He^* + C_2H_2$ case. For this interaction even dissociation combined with ionization of a molecular fragment molecule is possible. In both of these cases, Cermak's results indicate that the electrons produced have a broad energy distribution with several peaks rather than a definite energy as in the preceding cases. Although other measurements are not available for comparison with our results, there have been theoretical treatments of Penning ionization

14
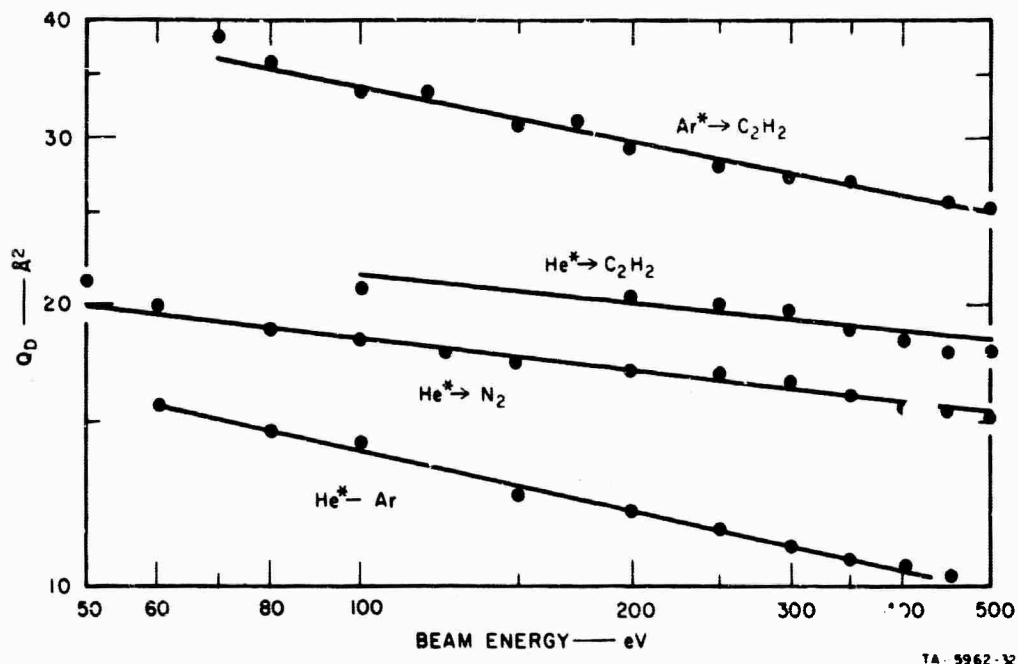
FIG. 5 DEACTIVATION CROSS SECTION AS A FUNCTION OF THE INCIDENT
BEAM ENERGY

processes. Katsuura[8] has calculated ionization cross sections for the
reactions

$$A* + B \rightarrow A + B^+ + e^-$$
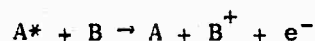
where the final states are located in a narrow region of the continuum.
This corresponds to our cases He* + Ar and Ar* + C_2H_2. For an interaction
potential $V(r) \sim r^{-6}$, where r is the internuclear distance of the colliding
particles, the slope of log Q_i^* vs log E (E is energy of the beam) should
be 0.2. This is in excellent agreement with our measurements. Watanabe
has theoretically investigated the case in which the final states are
located in a broad region of the continuum.[9] The reactions, He* + C_2H_2
and He* + N_2, probably fall in this category. With the interaction po-
tential $V(r) \sim r^{-6}$, the calculated slope of log $Q_i^* = \alpha$ log E should be
0.091. Again there is excellent agreement with our results. It must
be mentioned, however, that both theoretical papers assume that the op-
tical transition A* → A is allowed. A theoretical treatment by Ferguson[10]

15

lculating ionization cross sections by using a momentum transfer method predicts a slope of 0.33. This result does not agree with our measurement.

In the second group of measurements, the excitation energy of the metastable beam particles is lower than the ionization energy of the target gas. Figure 6 shows measurements where the target gas consists of the same kind of atoms as the beam particles. In these cases resonant excitation transfer is the dominant process $(Q_D \simeq Q*)$. If

$$Q* \gg Q_i^*$$

the calculated cross sections from our measurements will reflect Q* for energies for which

$$Q_i^* > Q_i^o$$

Because no measurements of Q* or Q_i^* are available, we assume that our approximations are valid and compare our results with theoretically expected results for resonant excitation transfer processes.[11,12] For these processes the well known relation

$$\sqrt{Q*} \sim \ell n(E)$$

should be valid. The plot of our measurements shows that the experimental values follow the theoretical law. Furthermore, in the case He* + He, absolute values for the excitation cross section Q* have recently been calculated by N. Lane[13] for beam energies up to about 100 eV. His preliminary results are in very good agreement with an extrapolation of our measurements toward lower energies.

The agreement between our measurements and the theoretically expected law in both cases and with calculated absolute values for Q* in the case He* + He seems to justify our approximations and the assumption that the measured cross section can be interpreted as the excitation transfer cross section.
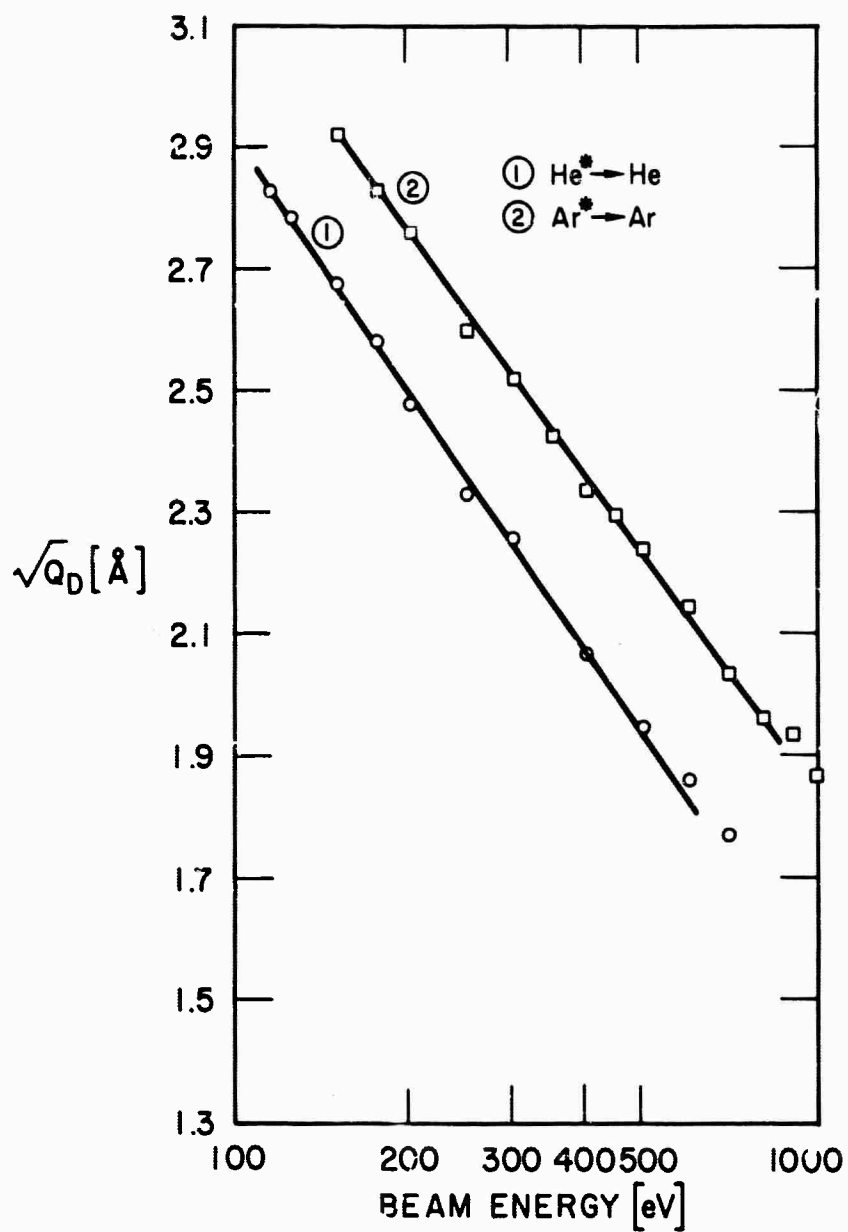
FIG. 6 DEACTIVATION CROSS SECTION AS A FUNCTION
OF THE INCIDENT BEAM ENERGY

TB-5962-25

17

5. Errors

The currents of the three operational amplifiers are scanned in less than 1/2 second. This reduces errors due to beam instabilities to a negligible amount. Each cross section is obtained from the average value of at least 30 scans at a fixed target gas pressure. This procedure is repeated for 6 to 10 different pressures which yield total attenuations over the range 5% to 50% when measured at the surface detector. The final cross section is the average of all cross sections. Over most of the pressure range the cross sections are fairly constant. The main error is due to a 5% to 10% increase of the apparent cross section at the low end of the pressure range, where the pressures are 1/4 to 1/5 the maximum. Error bars of ±10% include this systematic error as well as additional uncertainties connected with the electronic measurements.

6. Conclusion

Deactivation processes of metastable He and Ar atoms passing through various gases with energies from 50 to 1000 eV have been studied. When the deactivation is dominated by Penning ionization processes, two types of behavior can be distinguished. If the process predominantly involves excitation transfer to one state, the velocity dependence of the cross section is found to be $Q_i^* \propto v^{-2/5}$. If several states are involved in the transfer, $Q_i^* \propto v^{-1/5}$. Both of these results are consistent with available theory.

Because of the additional assumptions, the measured cross sections are less certain than the ionization measurements when the deactivation is due to symmetric energy exchange. However, they obey the relation $\sqrt{Q^*} \propto \ln(E)$ expected on theoretical grounds.

B. Studies of the Radiation Emitted from States Excited by Electron Capture Collisions

Measurements of the radiation emitted by excited states produced in asymmetric electron capture reactions were started last year. At the time of the last report,[1] spectra had been obtained from a number of reactants in order to determine the number and identity of excited states involved in a specific reaction. It had also been ascertained that the $C^3\Pi_u$ state of N_2 was produced when N_2^+ captured an electron from sodium. Earlier[2] we had measured the $N_2^+ + Na$ total charge transfer cross section and found it to exhibit a near-resonant energy dependence indicative of capture into the C state or some other nearby state.

This year the program has continued partly in this exploratory mood; the techniques have been extended to include a monochromator-phototube combination, and recently we have measured several cross sections (as a function of incident ion energy) for the production of specific lines and bands, using narrow pass band filters and a photomultiplier. This work will be described in greater detail in a technical report now being prepared. A brief summary is presented here.

1. Identification of the Radiative Transitions

Spectra arising from allowed transitions in the products of reactions between the ions He^+, Ar^+, and N_2^+ and a potassium vapor target were first examined with a grating spectrograph. A wavelength interval extending approximately from 3000 to 5000 Å was studied with a resolution of about 5 Å. These spectra gave information on the relative population of various excited states and also permitted the selection of several relatively isolated lines for cross section measurements using narrow band filters.

a. He⁺ + K

The emission spectrum obtained at 1470 eV incident He⁺ energy is shown in Fig. 7. He excitation from this reaction should occur largely to the n = 2 levels, but the allowed transitions from these states radiate at 584 or 10830 Å and thus were not observable. The only He line observed was at 3889 Å, from the $3p\,^3P$ state (ΔE = 2.75 eV). The 5876 emission from $3d\,^3D$ was probably present but was not recorded on the 103a-O film used.
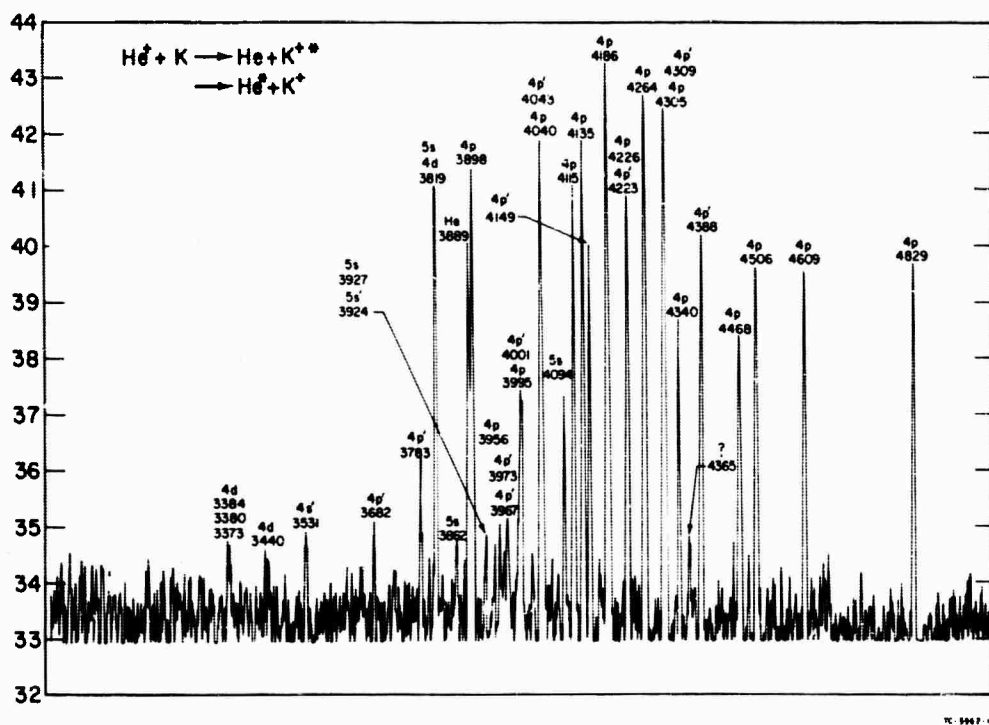
FIG.7   EMISSION SPECTRUM FROM He⁺ + K COLLISIONS AT 1470 eV

A number of lines from excited K⁺ states were observed. Reactions to these states can be near-resonant when the final He is in the ground state; however, the minimum $|\Delta E|$ for final states that radiate within our range of observation was about 3 eV. Most of the observed radiation came from these (4p) levels (Fig. 8).

20
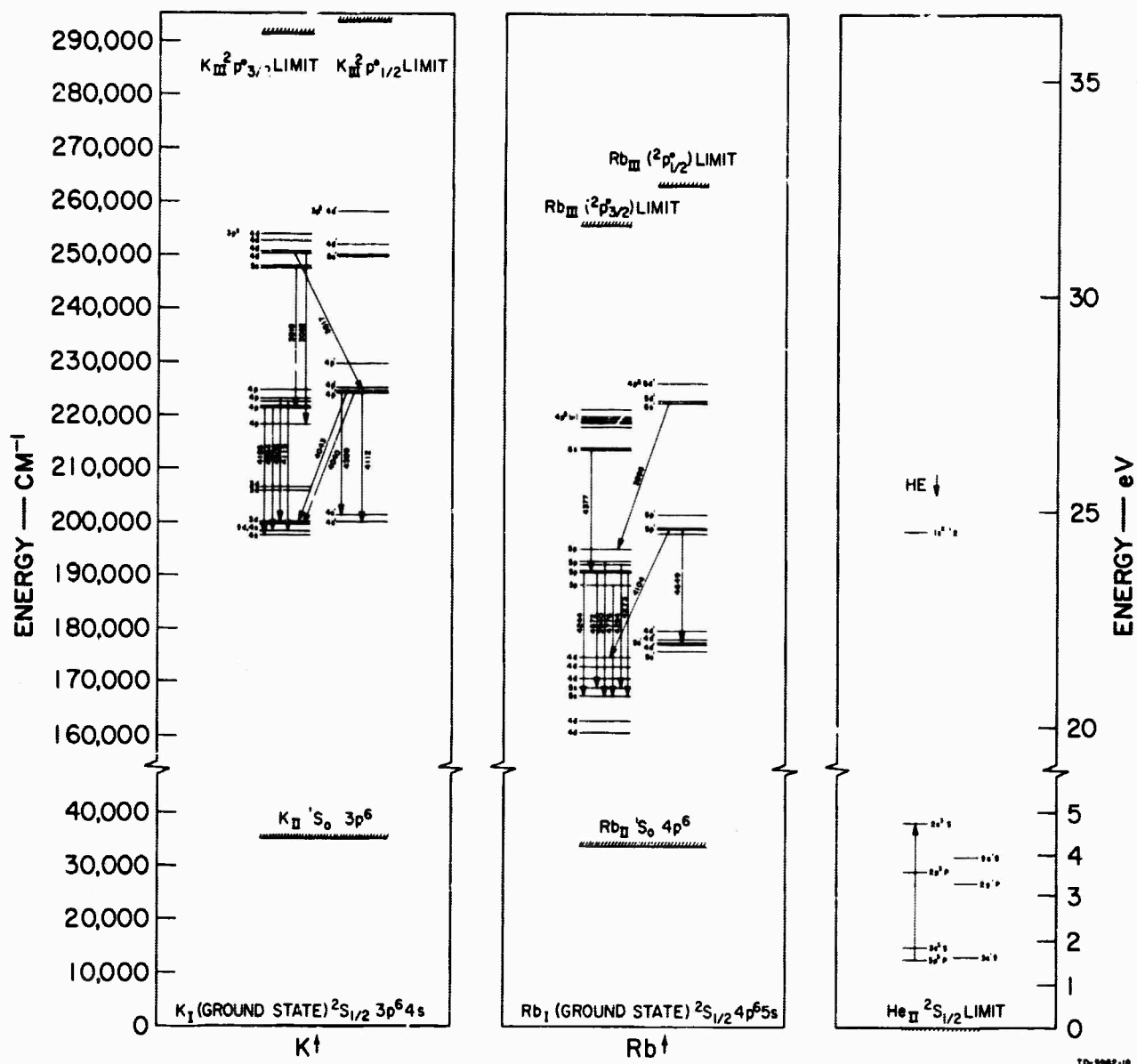
FIG. 8 IMPORTANT ENERGY LEVELS OF He, K AND Rb AND THEIR IONS
Direction of Increasing Energy is indicated by arrow alongside species symbol.

21

It is informative to compare the states populated in the He^+ + K reaction with the available states and their ΔE as in Fig. 8 (only the most important levels are included). The direction of increasing energy is given by the arrows near the species symbol, and the diagrams are juxtaposed so that the ground state He^+ level is next to the ground state K (and Rb) levels, representing the initial state of the system. Obviously, for a transition to the final state of He + K^+ to occur with no energy change, the final states will also lie at the same level. Thus if the final K^+ is in the ground state the reactions of smallest ΔE will leave the He atom in the 2^3S and 2^1S levels, and if the final He is in the ground state the K^+ atom is in the group of lowest excited ion states. Radiative transitions observed in our spectra are indicated by arrows.

b. Ar^+ (and Ar^{++}) on K

This case differs from that of He^+ because, while excited Ar states can be produced by near-resonant capture reactions, excited K^+ are unlikely because these reactions have ΔE's of at least 8 eV. In this case the primary radiation is probably in the ultraviolet lines resulting from capture into the resonance levels of Ar. The only lines observed were of ArII, excited in electron capture collisions of Ar^{++} (a contaminant in the beam) on K. This mechanism was verified by changing the ion source conditions so that no Ar^{++} ions were produced; the Ar^+ lines were no longer seen.

c. N_2^+ + K

These reactions were the most interesting ones that we have examined optically, for here we could observe the radiation from states of N_2 excited by near-resonant electron capture reactions. From a consideration of the energy levels of the reactants and products, one would expect to produce N_2 in the $C^3\Pi_u$ state ($\Delta E \approx 0$ for $v = 1$), which decays to $B^3\Pi_g$ in 4×10^{-8} sec, emitting the N_2 second positive bands.

22

Examination of the N_2^+ + K spectrum (Fig. 9) confirms the prediction. Only bands of the $N_2(2^+)$ system were observed. After the radiative transition, the final $B^3\Pi_g$ state subsequently cascades to the $A^3\Sigma_u$ state in $3\text{-}10 \times 10^{-6}$ sec, but the strong bands are in the infrared and thus were not seen. In any case, this reaction is apparently a good mechanism for providing beams of N_2 in the B and A states (with populations dependent on the time elapsed after neutralization of the ion beam).

2. Monochromator-Phototube Measurements

While the spectrograph provided adequate resolution for line identification, little could be done to establish meaningful relative intensities for the various lines because of the inherent nonlinearity of the film and the fact that the grating was blazed for 7500 Å, thus making the response a steep function of wavelength in the 3000-5000 Å region. A fairly fast (f/3.5) monochromator was obtained and used in conjunction with a cooled low noise EMI6256S photomultiplier, in hopes of providing reliable intensity data that could ultimately be used for cross section determinations. Without using pulse counting techniques, the system has insufficient sensitivity for operation at the lower ion beam energies where the beam current is small. However, the apparatus is useful in obtaining relative intensity measurements at beam energies over 1000 eV.

a. N_2^+ + K

Figure 10 shows several sections of the photomultiplier output trace in the wavelength range 2200 Å $< \lambda <$ 4000 Å where only the second positive bands of N_2 were found (the lack of other bands suggests preferential population of the $v' = 1$ level). These data were used as a standard to determine the relative magnitudes of all other observed bands. The overlap of some of the bands such as $(2,1)$ and $(3,2)$ was substantial and the unfolding was only approximate, but the results were quite satisfactory. To test the accuracy of these measurements and estimate the error made

23
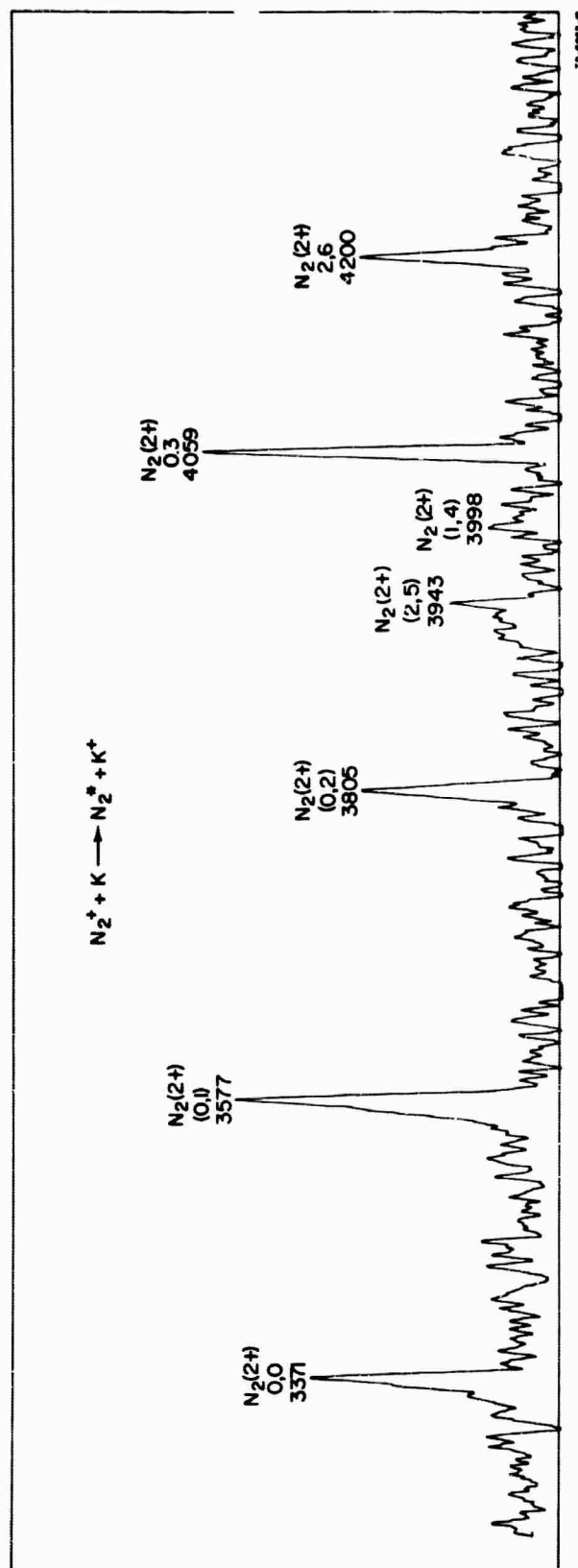
FIG. 9 EMISSION SPECTRUM FROM N_2^+ + K COLLISIONS AT 1500 eV
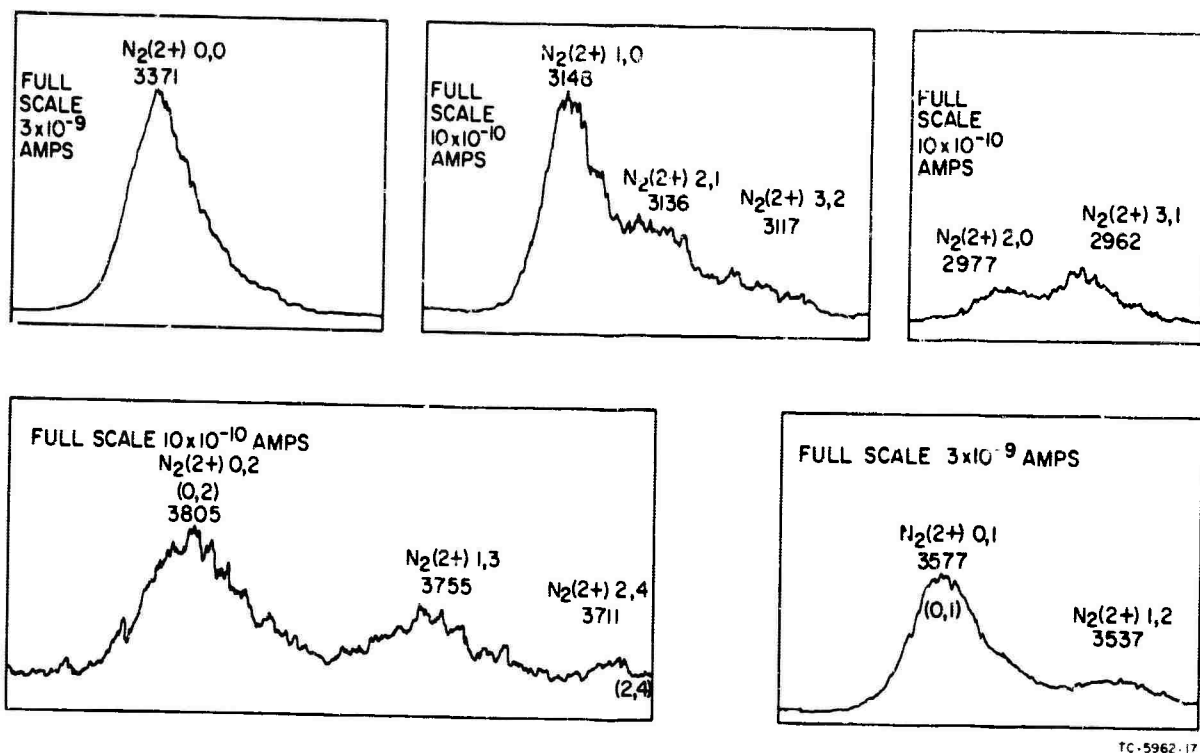
FIG. 10 SECTIONS OF THE MONOCHROMATOR SCAN OF SECOND POSITIVE BANDS EMITTED IN N_2^+ + K COLLISIONS AT 1400 eV

in assuming a flat wavelength-sensitivity curve for the photomultiplier, the branching of the radiation from a given upper state (v') level to several lower (v'') levels was compared to that predicted using the appropriate energy change and the Franck-Condon factors of Benesch et al.[14] The agreement was surprisingly good, considering the noise on the curve, and gave confidence in using the data for other comparisons. Summing over all peaks arising from the same upper vibrational level, we found the v' levels 0, 1, 2, and 3 to be populated in the relative amounts 10, 2.8, 0.9, and 0.6, respectively. This result shows that a $\Delta E = 0$ selection rule (which would predict an enhancement of the $v' = 1$ level) should not be construed to have much strength when possible final states differ in energy by a fraction of an electron volt. Other aspects of the interacting systems must be considered. In the present case, for instance, there is

25

undoubtedly a strong influence of the Franck-Condon overlap between the appropriate levels of $N_2^+(X)$ and the $N_2(C)$ states.

We found the intensities of the (0,2), (1,3), and (2,4) 2nd positive bands to be in the ratios 1.0:0.47:0.14, with the $N_2(C^3\Pi_n)$ state populated by electron capture collisions of N_2^+ and K, whereas the experimental values for excitation of ground state N_2 by electron impact are experimentally 1:0.84:0.44 (Langstroth's data in Craggs and Massey[15]) at electron energies above 30-50 eV and 1:0.70:0.18 for 15-keV electrons (Fishburne[16]). Representative theoretical values of 1:0.89:0.30 were reported by Fishburne[16] for electron impact excitation. Thus the particular electron capture reaction we used had the effect of populating the v = 0 level of the $N_2(C)$ state more heavily than is found from electron impact excitation of $N_2(X)$. The relative importance of the energy defect in determining this population, compared with that of the Franck-Condon factors, is unknown. A determination of the population distribution using other target atoms with different ionization potentials (such as Na or Rb) may shed some light on this question.

b. $\underline{NO^+ + K}$

It was expected that the $A^2\Sigma^+$ state of NO would be produced in this reaction. For ground state vibrational levels, the ΔE is about -0.6 eV. In the wavelength range 2200 Å $< \lambda <$ 4000 Å, only the NO γ bands that originate from the NO (A) state were observed. Furthermore, all the observed bands originate at the $v' = 0$ level of that state. The β bands originating from the "displaced" $B^2\Pi$ states were not observed at all, although the ΔE is nearly the same as the A state. This result clearly indicates the important role of the Franck-Condon principle in electron capture reactions.

3. Cross Section Measurements

Knowledge of the emission spectra obtained with the spectrograph and monochromator permitted the selection of several lines and bands sufficiently isolated so that narrow band pass filters could be used in conjunction with a photomultiplier to measure emitted flux densities without danger of contamination from other nearby lines. The detection efficiency was calibrated for each emission wavelength by means of a standard lamp and the transmission curve of the filter. So far, cross sections of three K^+ lines from $He^+ + K$ and three N_2^+ (2+) bands from $N_2 + K$ have been measured as a function of incident ion energy. The experimental arrangement is shown in Fig. 11. In these studies, none of the radiative lifetimes of states producing the observed radiation were comparable to the residence time of the appropriate particle in the region of observation; thus corrections for lifetime effects in the state populations or cross sections were not necessary.

Results for the $He^+ + K$ runs are shown in Fig. 12 (note that the 4189 cross sections have been multiplied by 1/10 in the figure). It should be mentioned that the most intense line examined, 4189 Å, is fed by the 3819 transition. We have not examined this aspect in detail. Using these cross sections it was possible to construct an approximate curve of relative intensity vs peak height for the densitometer traces of the spectrometer photographs. On the basis of these data, the cross section for exciting all K^+ states with $n > 3$ in the raction $He^+ + K \rightarrow K^+ + He$ was estimated to be 5.5×10^{-16} cm^2 (within a factor of 2) at 1500 eV. This is at least ten times smaller than the total $He^+ + K$ charge transfer cross section and reflects the fact that the $|\Delta E|$ is >3 eV for these reactions.

Cross sections for the $N_2(2+)$ $(0,0)$ and $(1,3)$ bands are shown in Fig. 13. Both of these cross sections exhibit the $Q^{1/2} = a - b \log E$ dependence characteristic of closely resonant electron capture reactions,

27
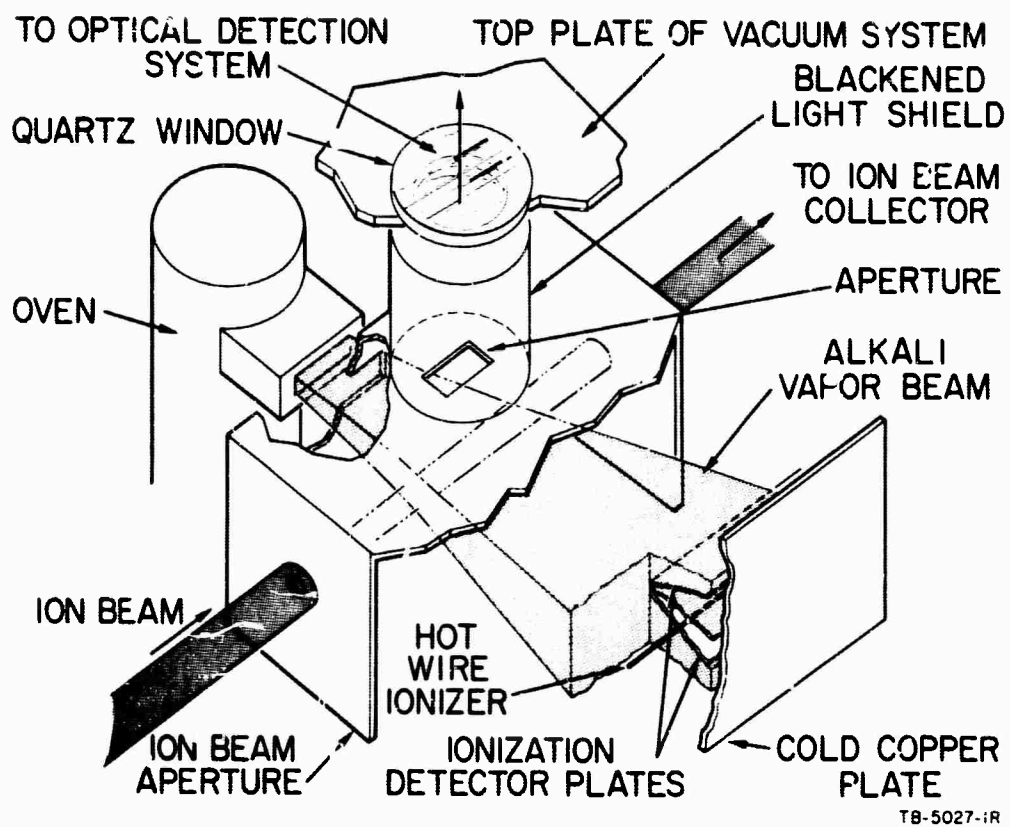
FIG. 11   EXPERIMENTAL ARRANGEMENT FOR THE EMISSION CROSS
SECTION MEASUREMENTS
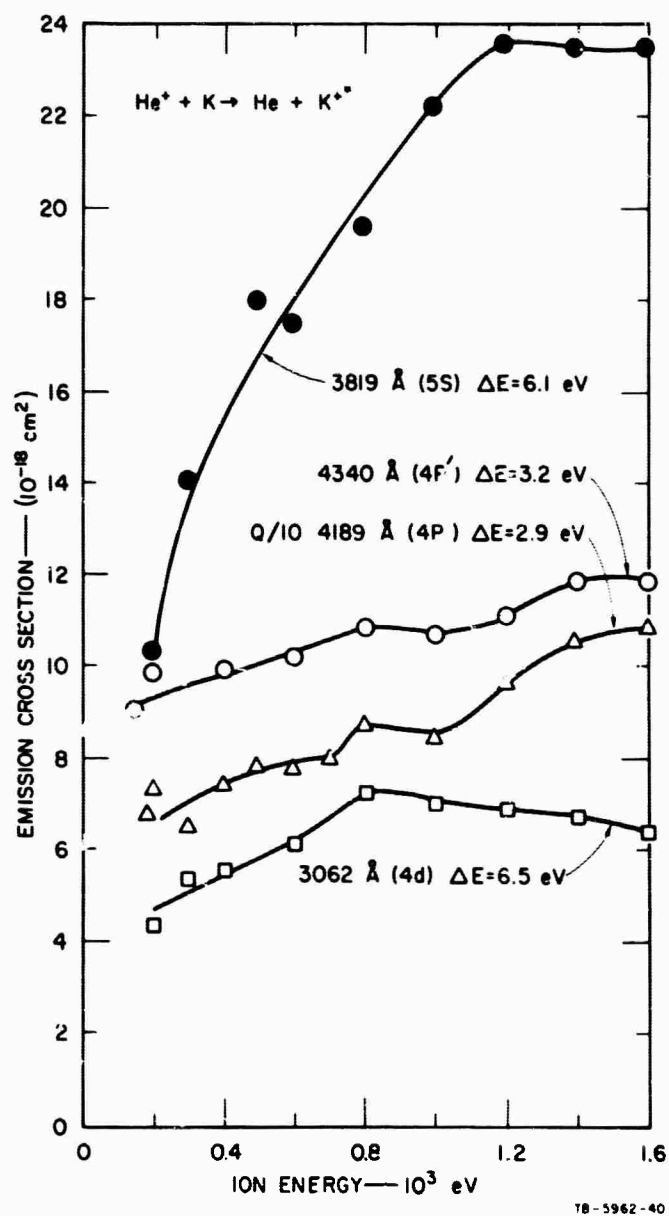
FIG. 12 EMISSION CROSS SECTIONS FOR SOME K II
LINES FROM He⁺ + K EMISSION
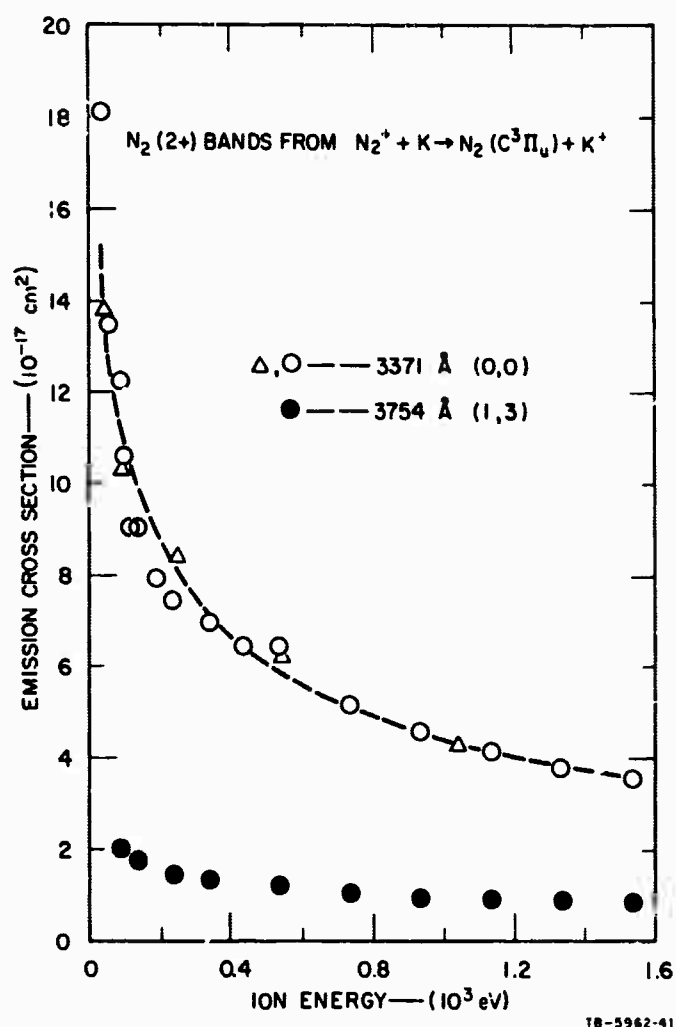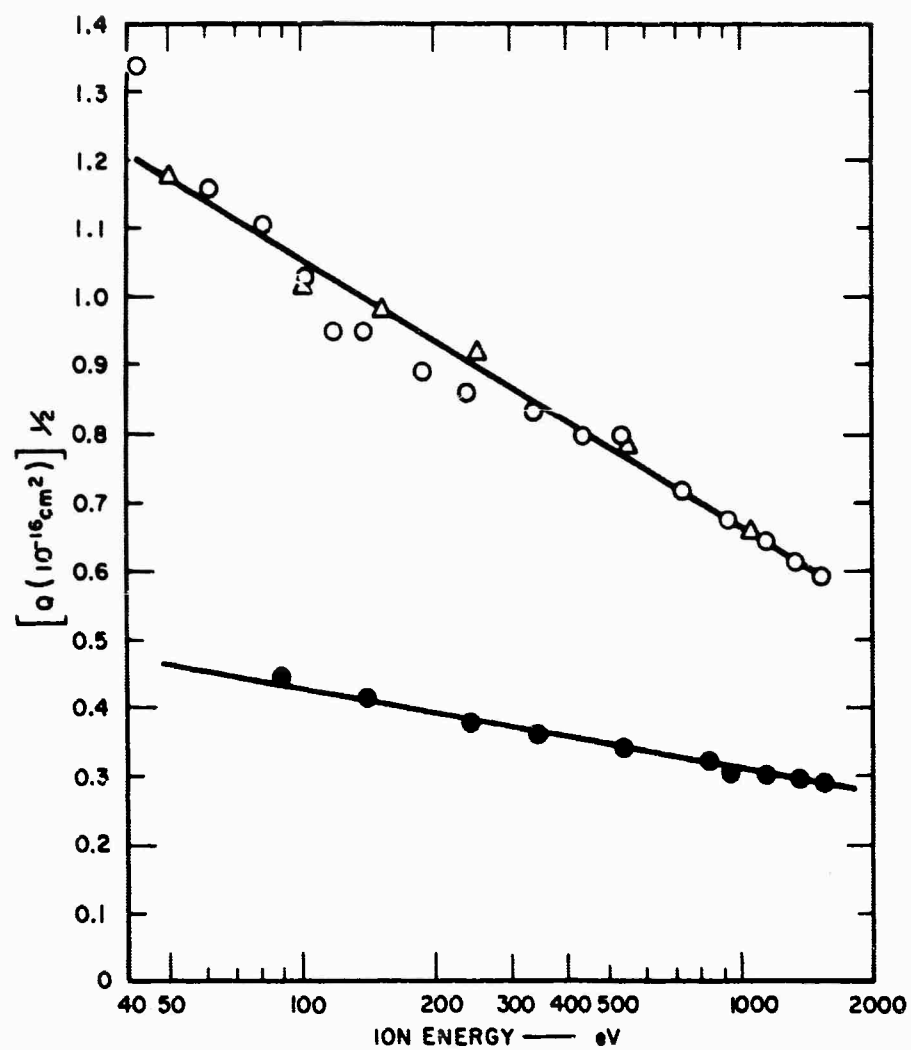
N_2 (2+) BANDS FROM $N_2^+ + K \rightarrow N_2 (C^3\Pi_u) + K^+$

$\triangle$, O ——— 3371 Å (0,0)

● ——— 3754 Å (1,3)

78-5962-41

FIG. 13 CROSS SECTIONS FOR THE 0,0 AND 1,3
SECOND POSITIVE BANDS FROM N_2^+ +
$K \rightarrow N_2^+ + K^+$

as can be seen in Fig. 14, which plots $Q^{1/2}$ vs log E. The dashed curve for the (0,0) band in Fig. 13 was taken from the straight line drawn through the data points in Fig. 14. Assuming that the relative population of the various vibrational levels of the $(C^3\Pi_u)$ state produced by electron capture is relatively independent of incident energy (the ratio of the (0,0) to (1,3) intensities ranged from 5.5 at 100 eV to 4 at 1500 eV), the monochromator spectrum taken at 1400 eV can be used to estimate the total cross section as a function of energy for exciting the N_2 $(C^3\Pi_u)$ state in the reaction $N_2^+ + K \rightarrow N_2^* + K^+$. This procedure gives a cross section about three times larger than that of the (0,0) band excitation cross section, and thus about 1/6 the total charge transfer cross section measured for $N_2^+ + Na$.

We have not yet measured the total $N_2^+ + K$ charge transfer cross section, but we feel that it should be at least as large as that for $N_2^+ + Na$. The $N_2^+ + Na$ cross section is presently somewhat uncertain. Our original estimated values[11] should be reduced by 50%, because the Na vapor pressure vs temperature curve used in estimating the cross section, taken from the tables of Ditchburn and Gilmour,[17] yields pressures that are 50% low, according to the more recent and accurate data of Buck.[18] Since our measurements of this cross section, another determination has been made by Henderson, Mentall, and Fite.[19] Their results, in the energy range 50-200 eV, are about 1/25 of ours. We feel our results are accurate to ±50% and cannot explain the discrepancy in the two measurements. We note that, using our Na cross sections, the C state capture is comparable for Na and K. It seems fairly important for us to measure the charge transfer cross section for $N_2^+ + K$ and to place our $N_2^+ + Na$ results on a reliable absolute scale, as well as to recheck the calibration of the photon detector.

TA-5962-42

FIG. 14 $Q^{1/2}$ vs log E FOR THE (0,0) AND (1,3) N_2(2 +) BANDS FROM N_2^+ + K → N_2^* + K^+. Triangle (0,0) data were taken with better ion beam focusing.

4. Summary

Spectra were obtained of the light emitted from the interaction of a gaseous ion $(He^+, Ar^+, Ar^{++}, N_2^+)$ beam and an alkali (K) vapor beam; these combinations should produce excited final states, after electron capture reactions, either of the type (1) $A^+ + B \rightarrow A* + B^+ + \Delta E$ (where ΔE is the energy defect) or of the type (2) $A^+ + B \rightarrow A + B^{+*} + \Delta E$. The spectra bore out this assumption (there was no direct excitation observed) and provided a basis for the selection of several lines sufficiently isolated that cross section measurements could be made using optical filters and a photomultiplier detector.

Cross sections were measured for three K^+ lines from reactions of type (2) whose $|\Delta E|$'s were over 3 eV. They were quite small compared to the total capture cross sections, and had the general appearance of most nonresonant excitation cross sections.

On the other hand, cross sections for excitation of two bands originating in the $C^3\Pi_u$ state of N_2 by the reaction $N_2^+ + K \rightarrow N_2^* + K^+$ $(\Delta E < 0.3$ eV) displayed an energy dependence characteristic of resonant electron capture reactions. From these results we can now derive the vibration distribution and intensity of the $N_2(A^3\Sigma)$ beam that results by cascading from the C state. The resonant electron capture reactions show a definite tendency to obey the Franck-Condon principle.

33

BLANK PAGE

II ENERGY TRANSFER AND OPTICAL EXCITATION

Simple molecules have many relatively low lying metastable excited states. This is particlarly true of those formed from O and/or N. Deposition of energy into the atmosphere, either by nuclear explosion, missile penetration, or such natural events as solar radiation absorption, produces significant numbers of simple molecules in metastable states.

When selective collisional processes occur, it is possible for metastable species to produce observable phenomena. These phenomena can be used to indicate the total energy deposited in the formation of those species (detected by emission spectra) which are also characteristic of the means of energy deposition.

During the present contract period, not yet completed, three metastable species of particular interest in the excitation of air, $O_2(b^1\Sigma)$, $O(^1D)$, and $N_2(A^3\Sigma_u^+)$, have been produced and their collisional deactivation, and the consequences of this deactivation, have been studied in considerable detail. For example, it has been shown that $N_2(A^3\Sigma_u^+)$ is extremely efficient in exciting NO, CO, and Hg, all of which emit their energy relatively rapidly. Hence their emission at unusually high intensities indicates not only their presence (as a consequence of energy deposition), but also the presence of $N_2(A^3\Sigma_u^+)$. The presence of $N_2(A^3\Sigma_u^+)$ is indicative of both the mode of energy injection into air and the quantity of energy involved.

Atomic oxygen becomes a major atmospheric species above 120 km and is a consequence of solar energy depostion in our atmosphere. Molecular oxygen absorption of ultraviolet solar radiation produces $O(^1D)$ as well as $O(^3P)$. The pathways by which the energy of excitation is degraded to thermal energy have important consequences for the composition and energy
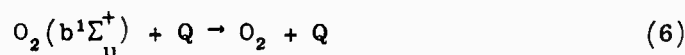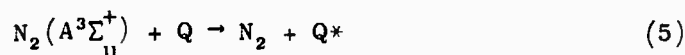
state of our upper atmosphere. We have found that $O(^1D)$ is strongly de-activated by O_2 (which is itself excited) and are attempting to determine the effectiveness of N_2 in removing energy from $O(^1D)$.

A. Method of Approach

Two experimental approaches are being successfully pursued. In one approach called, for convenience, the RF excitation experiment, highly purified gas at low pressure flows past several inlets (in a glass system) through a 5-liter quartz RF excitation bulb, through a 1-liter chemilumi-mescence observation bulb, and finally to a 1-liter/sec mechanical vacuum pump.

The gas is excited by a pulsed, high impedance (Tesla type) 150 kc/s oscillation and is observed with a filtered photomultiplier and two mono-chromators with photomultiplier detection. Steady state data (i.e., spectral scans, or variations of light intensity with power, or the con-centration of an additive) are recorded. Transient data (i.e., the build-up and decay of intensity as the excitation is keyed on and off) is stored digitally in a 1024-channel data accumulator. After sufficient repetitive cycles have occurred, the information is read out and photographed on an oscilloscope.

This experimental apparatus has successfully measured:

$$N_2\left(A^3\Sigma_u^+\right) + Q \rightarrow N_2 + Q \tag{4}$$

$$N_2\left(A^3\Sigma_u^+\right) + Q \rightarrow N_2 + Q* \tag{5}$$

$$O_2\left(b^1\Sigma_u^+\right) + Q \rightarrow O_2 + Q \tag{6}$$
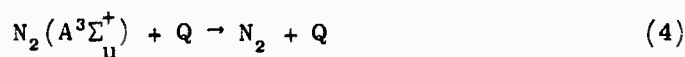
for a large selection of deactivators Q, ranging from N and O to O_2, N_2, NH_3, and Hg.

In the near future reactions such as (4), in which Q may be decomposed, will be studied and the fragments into which Q is broken will be identified and measured.

Studies of $O(^1S)$, OH*, and CN* will also be pursued. These species can be expected to result if hydrocarbons are present during energy desposition in the atmosphere.

A second experimental program, optical detection of photolysis fragments (ODPF), has yielded significant information on the behavior of $O(^1D)$ with O_2. However, success has not yet been achieved in direct detection of emission from $O(^1D)$ at 6300 Å.

Since the radiative lifetime of $O(^1D)$ is 100 sec, very sensitive detection, strong production rates, and minimal collisional deactivation are required. As it often turns out, these requirements are contradictory.

A new system for ODPF, which will make possible more complete observation of the phenomenon, is nearing completion. The new system has provision for subjecting the inflowing gas to a microwave discharge. In this way one (complex) radical can be injected by photolytic decomposition into a stream containing another. For example, chemionization due to

$$CH + O \rightarrow CHO^+ + e$$

$$CH* + O \rightarrow CHO* + e$$
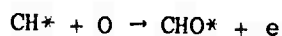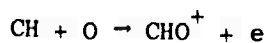
can be verified uniquely by forming CH or CH* in photolysis of a compound RCH, i.e.,

$$h\nu + RCH \rightarrow R + CH$$
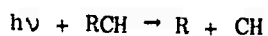
entrained in a gas stream containing O and observing coincident ionization.

Similarly, a study of the excitation of CN, OH, CH, etc., by energy transfer or reactions involving O, N, NO, N_2, or O_2 can be carried out. These experiments are in an advanced planning stage.

B. Detailed Discussion of Optical Detection of Photolytic Fragment Program

1. Excited Fragments

In principle, the ODPF is quite general and very informative. Radiation is absorbed by a gas S, giving excited fragments X* and unexcited fragments Y. Then the rate of production P(X*) is

$$P(X*) = \frac{\Phi(X*) I_{abs}}{V} \tag{7}$$

where Φ is the fraction of the photons absorbed that decompose into fragments, one of which is X* (i.e., Φ is the quantum yield for X* and is a function of the wavelength of the radiation used and the species absorbing the radiation). The volume of the vessel containing S is V, and X* is assumed to uniformly fill the container by diffusion. If this uniformity is not achieved, corrections are possible.

In a steady state

$$P(X*) = L(X*)[X*] \tag{8}$$

where L is the frequency of destruction of X* by all processes, including radiation. Since

$$I(X*) = \frac{[X*]}{\tau_r(X*)} \tag{9}$$

$$\frac{\Phi(X*) I_{abs}}{V} = P(X*) = L(X*)\tau_r(X*)I(X*) \tag{10}$$

The quantities $\Phi(X*)$ and $L(X*)\tau(X*)$ provide considerable information on the structure of S and the energy transfer processes involving X*.

38

One of two things can happen to X*; it can react and be removed as a chemical entity or it can be deactivated to X, but still retain its chemical identity. Then

$$L(X*) = L_o = k_R[Q] + k_Q[Q] \tag{11}$$

where [Q] is the concentration of a collision partner in reactive and energy transfer collisions, respectively. It is possible (and quite probable) for one species to produce both effects. Then

$$k_T = k_R + k_Q$$

where k_T is the total rate of removal of X* by Q. The term L_o lumps together processes not of immediate interest and necessarily includes radiation and reaction and/or quenching of X* by S, i.e.,

$$L_o = \frac{1}{\tau_r(X*)} + k_T'[S] + \ldots \tag{12}$$

Equation (10), after substitution of Eq. (11), becomes

$$\frac{\Phi(X*)I_{abs}}{VI(X*)} = L_o + k_T[Q] \tag{13}$$

If $\Phi(X*)$ is known and $I_{abs}/VI(X*)$ can be absolutely measured, L_o and k_T can be obtained from measurements of $I(X*)$ vs [Q]. Alternatively, if either L_o or k_T is known, it is possible to obtain $\Phi(X*)$.

2. Absolute Measurements Using Unexcited Photolysis Fragments

The problem is to obtain $I_{abs}/VI(X*)$ in absolute units. To indicate how such absolute measurements can be made, it is necessary to consider a specific experiment. If I_{abs}/V could be obtained from in situ emission measurements, then the absolute measurement would reduce to relative intensity measurements--a much more desirable situation.

39

It is possible to obtain I_{abs}/V from emission measurements by utilizing the photolysis of O_2 and the measurement of $O(^3P)$ by

$$NO + O \rightarrow NO_2 + h\nu$$
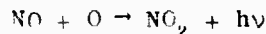
This reaction produces an extensive continuum from 400 to 1400 nm.

In general the rate of production of $O(^3P)$ is

$$P_3 = (\Phi_3 + \Phi_1 f) \frac{I_{abs}}{V} \tag{14}$$

where Φ_3 and Φ_1 are the quantum yield of $O(^3P)$ and $O(^1D)$ and f is the fraction of $O(^1D)$ that is deactivated to $O(^3P)$. This latter fraction is

$$f = \frac{L'_o + k_Q[Q]}{L_o + k_T[Q]} \tag{15}$$

where L'_o accounts for all processes that deactivate $O(^1D)$ to $O(^3P)$ except those involving Q.

For O_2 photolysis, it is known that f is 1 for experimentally useful situations and it is also known that at 1470 Å $\Phi_1 = \Phi_3 = 1$. Hence for O_2 photolysis at this wavelength,

$$P_3 = \frac{2I_{abs}(O_2)}{V} \tag{16}$$

where

$$I_{abs} = I_o\{1 - \exp(-\sigma_{O_2}[O_2]d)\} \tag{17}$$

σ_{O_2} is the absorption coefficient for O_2 at 1470 Å, $[O_2]$ the concentration of O_2 used, d the length of the absorption region, and I_o the intensity of the photolysis lamp. Since

$$\frac{I_{abs}(S)}{V} = \frac{I_{abs}(O_2)}{V} \left\{ \frac{1 - \exp(-\sigma_s[S]d)}{1 - \exp(-\sigma_{O_2}[O_2]d)} \right\} \tag{18}$$

$I_{abs}(S)$ is derivable from measurement of $P_3(O_2)$.

Again, for O_2 photolysis with added NO at steady state,

$$P_3 = \left\{ L_o(O) + k_A[NO][M] \right\} [O(^3P)]$$ (19)

where k_A refers to

$$NO + O + M \rightarrow NO_2 + M$$ (A)

which predominates over

$$NO + O \rightarrow NO_2 + h\nu$$ (B)

and $L_o(O)$ accounts for all other losses of $O(^3P)$. Also

$$I_B = k_B[NO][O] = \frac{k_B[NO]P_3}{L_o(O) + k_A[NO][M]}$$ (20)

so that for sufficiently large NO, I_B becomes constant at

$$I_B' = \frac{k_B P_3}{k_A[M]} = \frac{k_B \, 2I_{abs}(O_2)}{k_A[M]V}$$ (21)

It is now evident that

$$\frac{I_{abs}(S)}{V} = I_B'(O_2) \frac{k_A[M]}{k_B} \left\{ \frac{1 - \exp(-\sigma_s[S]d)}{1 - \exp(-\sigma_{O_2}[O_2]d)} \right\}$$ (22)

and so

$$\frac{I_B(O_2)\Phi(X*)}{I(X*)} \left\{ \frac{k_A[M]\{1 - \exp(\sigma_s[S]d)\}}{k_B\{1 - \exp(\sigma_{O_2}[O_2]d)\}} \right\} = \frac{I_B'(O_2)\Phi(X*)G}{I(X*)}$$
$$= L_o + k_T[Q]$$ (23)

Since the quantities in the large brackets, designated G, are all known, only the ratio $I_B'(O_2)/I(X*)$ needs to be measured and geometrical and detector sensitivity factors will cancel out, i.e., $I_B'(O_2)$ and $I(X*)$ can be replaced by $J_B'(O_2)$ and $J'(X*)$, the detection outputs, i.e.,

41

$$\frac{J'_B(O_2)\Phi(X*)G}{J_B(X*)} = L_o + k_T[Q] \tag{24}$$

If $\Phi(X*)$ is known, then varying $[Q]$ and plotting the left side of this equation against $[Q]$ gives k_T.

3. Photolysis Giving $O(^3P)$ and/or $O(^1D)$

Notice that if some other compound S' gives both $O(^3P)$ and $O(^1D)$ by photolysis, then

$$I'_B(S') = \frac{k_3}{k_A[M]} \ (\Phi'_3 + \Phi'_1 f) \ \frac{I_{abs}(S')}{V}$$

$$= (\Phi'_3 + \Phi'_1 f) I'_B(O_2) \ \frac{1 - \exp(-\sigma_s[S'])}{1 - \exp(-\sigma_{O_2}[O_2]d)} \tag{25}$$

$$= I'_B(O_2)(\Phi'_3 + \Phi'_1 f)G \ \frac{k_B}{k_A[M]}$$

So,

$$\frac{I'_B(S')}{I'_B(O_2)} = \frac{k_B}{k_A[M]} \ G(\Phi'_3 + \Phi'_1 f) \tag{26}$$

$$= G'(\Phi'_3 + \Phi'_1 f) \tag{27}$$

and G' can be easily calculated.

4. Photolysis and Reactions of N_2O

O_2 is a very efficient deactivator of $O(^1D)$, and N_2O is thought to react very rapidly with $O(^1D)$,

$$O(^1D) + N_2O \rightarrow N_2 + O_2 \tag{C}$$

42

while $O(^3P)$ is known not to react with N_2O. Then $f \approx 1$ in pure O_2 (with an inert buffer gas, He or Ar), but as N_2O is added $f \to 0$, i.e.,

$$f = \frac{k_Q[O_2]}{L_o + k_T[O_2] + k_c[N_2O]} \qquad (28)$$

When

$$k_c[N_2O]_{1/2} = L_o + k_T[O_2]$$

the continuum plateau intensity is halfway to the intensity characteristic of $f = 0$. Hence if $L_o \ll k_T[O_2]$, then

$$\frac{k_c}{k_T} = \frac{[O_2]}{[N_2O]} \qquad (29)$$

There are several barriers to applying this simple technique that are just now being removed. First, N_2O is decompos ' by emission at 1470 Å into fragments that lead to emission. Using our newly developed image tube spectrcgraph, we have detected emission from NO and $O(^1S)$ that overlaps the NO_2 continuum and requires careful filtering of the photomultiplier detectors used to measure I'_B if this unwanted emission is to be excluded.

After proper segregation of emission from NO_2 is accomplished, a correction must still be made for the production of $O(^3P)$ from N_2O, i.e.,

$$I'_B(O_2 + N_2O) = \frac{1}{V}\left\{ I_{abs}(O_2)[\Phi_3(O_2) + f\Phi_1(O_2)] \right.$$
$$\left. + I_{abs}(N_2O)[\Phi_3(N_2O) + f\Phi_1(N_2O)] \right\}$$

If $\Phi_1(N_2O) = 0$, it is relatively easy to carry out the appropriate correction. However, preliminary results suggest that this is not true and a study of $\Phi_1(N_2O)$ is required.

43

Equation (26) relates the intensity of the N_2O correction (at its plateau value) to Φ and f. However, $I_B'(N_2O)$ does not reach a plateau as NO increases (and N_2O stays fixed) as is the case with O_2. Since from the O_2 results we know that [NO] has reached a value where it dominates the processes removing $O(^3P)$ and hence cancels the [NO] in $I_B = k_B[NO][O]$, the increasing $I_B'(N_2O)$ can only imply that f is increasing and hence that $\Phi_1 \neq 0$.

Including the role of NO in f gives

$$f = \frac{L_o' + k_{NO}'[NO]}{L_o + k_{NO}[NO]}$$

Since L_o includes $k_{N_2}[N_2O]$, which is very large, while L_o' is very small (because N_2O reacts mostly with $O(^1D)$), then $L_o' < k_{NO}'[NO]$ while $L_o \gg k_{NO}[NO]$, i.e.,

$$f \approx \frac{k_{NO}[NO]}{L_o}$$

Therefore

$$\frac{I_B'(N_2O)}{I_B'(O_2)} = G'\left(\Phi_3 + \Phi_1 \frac{k_{NO}[NO]}{L_o}\right) = G'(\Phi_3 + \Phi_1)\frac{k_{NO}[NO]}{k_{N_2O}[N_2O]}$$

It must be remembered that G' is a known function of

$$[N_2O]\Big\} \propto \{1 - \exp(-\sigma_{N_2O}[N_2O]d)\}\Big\}$$

A similar effect does not occur for O_2 photolysis because $k_{O_2}'[D_2] \gg k_{NO}'[NO]$, while in N_2O photolysis $k_{N_2O}'[N_2O] \ll k_{NO}'[NO]$.

Preliminary results indicate that Φ_3 is quite small and $\Phi_1 \approx 1$. If this should be the case, then addition of a strong quencher, perhaps N_2

would give

$$\frac{I_B'(N_2O)}{I_B'(O_2)} = G' \left\{ \Phi_3 + \Phi_1 \frac{(k_{NO}'[NO] + k_{N_2}'[N_2])}{k_{N_2O}[N_2O]} \right\},$$
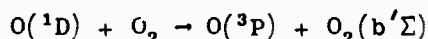
and, if $\Phi_3 \approx 0$ when $I_B'(NO)$ has been reduced to one-half its original value by N_2 addition,

$$k_{NO}'[NO] = k_{N_2}'[N_2]_{1/2}.$$

Stu..ies of the reaction and quenching of $O(^1D)$ and $O(^1S)$ by several interesting and important species can be carried out in a manner very similar to that already discussed.

C. Present Position of ODPF Experiments

We have established that

$$O(^1D) + O_2 \rightarrow O(^3P) + O_2(b'\Sigma)$$

occurs with a rate coefficient greater than 10^{-12} cm^3/sec. This result will soon be published in the Journal of Chemical Physics.

We have made extensive measurements of $O(^3P)$ resulting from O_2 and N_2O photolysis, as just discussed, and obtained results in general agreement with expectations. However, we have also discovered that results with relative precision of $\approx 1\%$ are required for accurate analysis. At this level of accuracy we find that surface phenomena are quite significant. We are now coating the walls of the photolysis bulb with inhibitors to reduce the reaction of $O(^3P)$ on the surface. Also, a second photomultiplier has been installed to observe the photolysis region with geometry significantly different from that in the previous detector. It is expected that results of sufficient precision will be obtained to measure Φ_1, Φ_3 of N_2O, and the rates of reaction of $O(^1D)$ with N_2O and CO_2 will be measured relative to the rate of quenching by O_2 and N_2.

45

D. RF Excitation Experiments

Let the excitation rate of some species, X, in the electrical discharge be P(X*); then

$$\frac{d[X*]}{dt} = P(X*) - L(X*)[X*] = P(X*) - L(X*)\tau(X*)I(X*). \qquad (30)$$

This equation is essentially the same as that used in discussing ODPF with the same meaning attached to the symbols $L(X*)$, $\tau(X*)$, $I(X*)$, and $[X*]$. In a steady state

$$P(X*) = L(X*)\tau(X*)I(X*)$$

Breaking $L(X*)$ into two components,

$$L(X*) = L_o(X*) + k_Q[Q]$$

and associating $I_o(X*)$ with the circumstance $[Q] = 0$, one can easily derive the equation

$$\frac{I_o}{I} = 1 + \frac{k_Q[Q]}{L_o(X*)}$$

provided that $P(X*)$ is not affected by the addition of Q. Hence a plot of I_o/I vs $[Q]$ gives $k_Q/L_o(X*)$.

Equation (30) can be rewritten as

$$\frac{dI(X*)}{dt} = \tau(X*)P(X*) - L(X*)I(X*)$$

If $P(X*)$ is a square pulse, i.e.,

$$P(X*) = 0 \text{ for } t < 0 \text{ and } P(X*) = P_o \text{ for } 0 \leqq t \leq t_1$$

46

then the solution of this equation is

$$I(X^*) = 0 \text{ for } t < 0$$

$$I(X^*) = I_s\{1 - \exp[-L(X^*)t]\} \text{ for } 0 < t < t_1$$

$$I(X^*) = I_s\{1 - \exp[-L(X^*)t]\}\exp[-L(X^*)t] \text{ for } t > t_1$$

$$I_s(X^*) = \frac{\tau(X^*)P(X^*)}{L(X^*)}$$

A steady state is reached when $t \approx 2/L(X^*)$. Hence if $P(X^*)$ is not constant but changes only slowly [i.e., $\approx$ 10-80% in a time interval of $2/L(X^*)$], then $I(X^*) \approx I_s(X^*) \propto P(X^*)$.

If $\ln I(X^*)$ is plotted vs t, the resulting straight line should have a slope of $L(X^*)$. Hence if this slope is plotted as a function of gas stream component $[Q]$ and $L(X^*) = L_0(X^*) + k_Q[Q]$, then a straight line results whose slope is k_Q.

We have detected, by emission, $O(^3S)$ (5577 Å), $O_2(b^1\Sigma)$ (7618 Å), $N_2(A^3\Sigma_u^+)$ (2800-3000 Å) and have investigated the changes in the transient behavior of their emission as $[Q]$ is added.

Several papers concerning $N_2(A^3\Sigma_u^+)$ interaction with N, NO, and Hg are in the process of publication, and a final draft of a survey paper covering all the species listed is near completion.

BLANK PAGE

III FIELD OBSERVATIONS OF UPPER ATMOSPHERIC PHENOMENA

The objective of the work reported here is to obtain spectra of radia-
tion associated with high altitude release of barium and strontium. The
experiment was conducted during the nights of October 3 and 4, 1967; the
rockets carrying the release material were launched from the Wallops
Island range, and the optical equipment was set up at Langley Air Force
Base.

The basic equipment used was a transmission spectrograph system
employing an image intensifier tube and a unique spectrograph (owned by
SRI) employing all reflecting optics for use in the ultraviolet region
of the spectrum. It was necessary to modify both instruments before they
could be used on this project.

A. Instrument Modifications

The UV spectrograph had no easy means for adjusting the angle of
sight. Si e this spectrograph is fairly heavy (about 400 pounds), a
set of steerable mirrors in front of the slit were installed. This spec-
trograph is designed to use an echelle grating and a second grating ori-
ented with its ruling perpendicular to those on the echelle grating to
separate its overlying diffraction orders. The despersion is about 12 $\overset{\circ}{A}$/mm
at 4000 $\overset{\circ}{A}$. Since the echelle grating spreads the light into several orders,
the optical speed of the instrument is less than if a single grating were
used; but, of course, the dispersion is greater. The echelle grating was
replaced with a plane mirror giving an increase in speed of about a factor
of three but reducing the dispersion to about 80 $\overset{\circ}{A}$/mm. For the barium-
strontium experiment it was felt that speed was more important than res-
olution, and the spectrograph was used with the echelle grating removed.

Luminous spots formed by the Ba-Sr release grow rapidly to a size that is too large to obtain good data from an objective spectrograph. It was therefore necessary to put a slit and collimator on the image tube unit to convert it to a standard slit spectrograph. Based on the information we had as to the size the spots attained and the accuracy of the release, a collimator was chosen that would give a wide 20-degree field of view.

B. Results

At the present time data reduction has just started; however, a few general comments can be made. The all-reflecting ultraviolet spectrograph detected only one line at 4607 Å the first night; on the second night an additional line was observed at 4554 Å. The 4607 Å line was observed for 116 sec the first night and 266 sec the second night. The 4554 Å line was seen the second night 1166 sec after launch.

Because of the lack of experience with the instrument and the lack of an adequate check list, an adjustable iris diaphragm which was closed during the day to protect the image intensifier tube was left closed during the first night's run and most of the second night. This error was detected late in the second night's run. Spectra containing several lines and bands were obtained using 10-sec exposures 26 minutes into the second night's run.

REFERENCES

1. D. C. Lorents and J. R. Peterson, "Research on Metastable Species in Atomic and Molecular Beams Produced by Charge Transfer", Semi-Annual Report, Sponsored by ARPA, Project Defender, U.S.A.R.O. Durham Contract DA-31-124-ARO-D-446, Oct. 31, 1966.

2. D. C. Lorents and J. R. Peterson, "Research on Metastable Species, in Atomic and Molecular Beams Produced by Charge Transfer, Final Report, Sponsored by ARPA, Project Defender, U.S.A.R.O. Durham Contract DA-31-124-ARO-D-220, Sept. 20, 1965.

3. B. L. Donnally, T. Clapp, W. Sawyer, and M. Schultz, Phys. Rev. Letters $\underline{12}$, 502 (1964).

4. D. C. Lorents and W. Aberth, Phys. Rev. $\underline{139}$ A1017 (1965).

5. M. Hollstein and H. Pauly, Phys. $\underline{196}$, 353, (1966).

6. H. C. Hayden and N. G. Utterback, Phys. Rev. $\underline{135}$(6A), A1575 (1964).

7. V. Cermak, J. Chem. Phys. $\underline{44}$, 3774, (1966).

8. K. Katsuura, Chem. Phys. $\underline{42}$(1), 3771 (1965).

9. T. Watanabe, Chem. Phys. $\underline{46}$(10), 3741 (1967).

10. E. E. Ferguson, Phys. Rev. $\underline{128}$, 210 (1952).

11. B. M. Smirnov and O. B. Firsov, JETP Pis'ma $\underline{2}$, 478, (1965).

12. B. M. Smirnov, JETP, $\underline{51}$, 466 (1966).

13. N. Lane, private communication.

14. W. Benesch, J. T. Vanderslice, S. G. Tilford, and P. G. Wilkinson, Astrophys. J. $\underline{144}$, 408 (1966).

15. J. D. Craggs and H. S. W. Massey, in Handbuck der Physik, S. Flügge, Ed. (Springer Verlag, Berlin, 1955), Vol. 37, Pt. 1., p. 337.

16. E. S. Fishburne, J. Chem. Phys. <u>47</u>, 58 (1967).

17. R. W. Ditchburn and J. C. Gilmour, Rev. Mod. Phys. <u>13</u>, 310 (1941).

18. U. Buck, Diplom Thesis, Institut für angewandte Physik der Universität Bonn, 1965 (to be published).

19. W. R. Henderson, J. E. Mentall, and W. L. Fite, J. Chem. Phys. <u>46</u>, 3447 (1967).

STANFORD RESEARCH INSTITUTE ⊛SRI

Main Offices and Laboratories

333 Ravenswood Avenue
Menlo Park, California 94025
(415) 326-6200
Cable: STANRES, Menlo Park
TWX: 910-373-1246

Regional Offices and Laboratories

Southern California Laboratories
820 Mission Street
South Pasadena, California 91030
(213) 799-9501 • 682-3901

SRI-Washington
1611 North Kent Street, Rosslyn Plaza
Arlington, Virginia 22209
(703) 524-2053
Cable: STANRES, Washington, D.C.

SRI-New York
200 E. 42nd Street
New York, New York 10017
(212) 661-5313

SRI-Huntsville
Missile Defense Analysis Office
4810 Bradford Blvd., N.W.
Huntsville, Alabama 35805
(205) 837-3050
TWX: 810-726-2112

SRI-Chicago
10 South Riverside Plaza
Chicago, Illinois 60606
(312) 236-6750

SRI-Europe
Pelikanstrasse 37
Zurich, 8001, Switzerland
27 73 27 or 27 81 21
Cable: STANRES, Zurich

SRI-Scandinavia
Skeppargatan 26
Stockholm Ö, Sweden
600-226; 600-396; 600-475

SRI-Japan
Edobashi Building, 8th Floor
1-6, Nihonbashi Edobashi
Chuo-ku, Tokyo
Tokyo 271-7108
Cable: STANRESEARCH, Tokyo

SRI-Southeast Asia
Bangkok Bank Building
182 Sukhumvit Road
Bangkok, Thailand
Bangkok 910-181
Cable: STANRES, Bangkok

Representatives

Canada
Cyril A. Ing
86 Overlea Boulevard
Toronto 17, Ontario, Canada
(416) 425-5550

Italy
Lorenzo L. Franceschini, Representative
Via Macedonio Melloni 49
Milan, Italy
72 32 46

Philippines
Roland H. Alm
The Gilarmi Apartments
Makati, Rizal, Philippines

Portugal
Eng. J. Gasparinho Correia
Avenida João XXI, 22-3° Esq.
Lisbon, Portugal
72 64 87

DOCUMENT CONTROL DATA - R & D

(Security classification of title, body of abstract and indexing annotation must be entered when the overall report is classified)

1. ORIGINATING ACTIVITY (Corporate author)	2a. REPORT SECURITY CLASSIFICATION
Stanford Research Institute	Unclassified
	2b. GROUP NA

3. REPORT TITLE

RESEARCH ON METASTABLE SPECIES IN ATOMIC AND MOLECULAR BEAMS PRODUCED BY CHARGE TRANSFER, Tasks I, II, and III

4. DESCRIPTIVE NOTES (Type of report and inclusive dates)

Technical Report

5. AUTHOR(S) (First name, middle initial, last name)

Hollstein, M.   Peterson, J. R.
Lorents, D. C.   Young, R. A.

6. REPORT DATE	7a. TOTAL NO. OF PAGES	7b. NO. OF REFS
27 December 1967	63	19

8a. CONTRACT OR GRANT NO.	9a. ORIGINATOR'S REPORT NUMBER(S)
DA-31-124-ARO-D-446	SRI Project PAU-5962
b. PROJECT NO. ARPA ORDER NO. 553	
c.	9b. OTHER REPORT NO(S) (Any other numbers that may be assigned this report) 5134.5-P
d.	

10. DISTRIBUTION STATEMENT

This document has been approved for public release and sale; its distribution is unlimited.

11. SUPPLEMENTARY NOTES	12. SPONSORING MILITARY ACTIVITY
None	U.S. Army Research Office-Durham Box CM, Duke Station Durham, North Carolina 27706

13. ABSTRACT

Excited Species and excited state reactions involving radiative and metastable states of atmospheric species play an important role in reentry physics. Progress in laboratory studies leading to the understanding of these reactions and the determination of the pertinent reaction rates is reported. Near-resonant electron capture reactions are being used to produce beams of long-lived excited atoms and molecules (metastables) suitable for studies of important collision processes of such species. The research has progressed sufficiently to allow the measurement of cross sections as a function of kinetic energy for metastable deactivation processes. Reactions in which the deactivation was dominated by Penning ionization or by symmetric energy transfer were chosen for study so that cross sections for these particular processes could be obtained. Studies of the optical radiation emitted from states excited by electron capture collisions have also provided useful results. In particular, cross sections for electron capture into the $v' = 0, 1, 2$ vibrational levels of the $C^3\Pi_u$ state of N_2 have been measured as a function of energy for the reactants $N_2^+ + K$, by observing the second positive radiation.

14. KEY WORDS

metastable states of atmospheric species
excited state reactions
optical radiation
cascade radiation

DD FORM 1473 NOV 65   REPLACES DD FORM 1473, 1 JAN 64, WHICH IS OBSOLETE FOR ARMY USE.